

# Microstructure-based computational simulation and experimental measurement of stresses in spheroidized steels

メタデータ	言語: eng 出版者: 公開日: 2017-10-03 キーワード (Ja): キーワード (En): 作成者: メールアドレス: 所属:
URL	<a href="http://hdl.handle.net/2297/16825">http://hdl.handle.net/2297/16825</a>

# Microstructure-based Computational Simulation and Experimental Measurement of Stresses in Spheroidized Steels

Lei Che<sup>1, a</sup>, Masahide Gotoh<sup>2, b</sup>, Yoshiaki Horimoto<sup>1, c</sup> and Yukio Hirose<sup>2, d</sup>

<sup>1</sup> Graduate school, Kanazawa University, Kanazawa, 920-1192, Japan

<sup>2</sup> Kanazawa University, Kanazawa, 920-1192, Japan

<sup>a</sup> che@cs.s.kanazawa-u.ac.jp, <sup>b</sup> masahide@cs.s.kanazawa-u.ac.jp

<sup>c</sup> y\_ho@zpost.plala.or.jp, <sup>d</sup> hirose@kenroku.kanazawa-u.ac.jp

**Keywords:** Stress, X-ray, simulation, microstructure-based, cementite, multiphase, steel

**Abstract.** Carbon steel is the most popular engineering material, usually consisted of ferrite and cementite phases. Internal stress state of the steel under thermal or mechanical loading is strongly affected by the amount and morphology in the cementite phase. With this aim, a computational model which applies the finite element method at the microscale was used in present study. Effects of volume fraction and particle size of the spheroidal cementite on the internal stress states in carbon steels under the mechanical and thermal loadings are investigated. To verify the reliability of the computational simulations, the residual stresses in the constituent phases are measured by means of X-ray stress diffraction technique. The computational simulations fit well with the experimental data, and the microstructure-based model is validated.

## Introduction

Cementite is one of the most well known metastable phases in carbon steels [1]. It forms either from austenite during cooling or from martensite during tempering. It mixes with ferrite, the other product of austenite, to form lamellar structures called pearlite and bainite. It has been introduced in previous studies that microstructural features of cementite particles have obvious effects on the internal stresses generated during the plastic deformation of steels, and the stress states are attributed to the inhomogeneous mechanical properties of steels [2, 3]. Lee *et.al* [4] have evaluated the effects of the carbon content, strain rate and temperature on the mechanical responses of the steels and found that an increase of carbon content enhanced the dynamic flow resistance of steels. da Silva *et.al* [5] have investigated the effect of the volume fraction of eutectic carbides on the thermal fatigue resistance of multi-component white cast iron and found that the surface crack density increased slightly for increasing volume fraction of eutectic carbides. It is concluded from these studies that the microstructural feature of cementite also affects strongly on the thermo-mechanical property of carbon steels. However, the stress evolutions of steels under the thermo-mechanical loadings are difficult to be investigated because of limitations of stress measurement instruments. Furthermore, it is impossible to independently vary the various microstructural parameters and thus isolate their effects on stress evolutions.

This study attempts to independently quantify the effect of particle size and volume fraction of the cementite on the internal stress states of steels under the mechanical and thermo-mechanical loadings using finite element analysis.

## Experimental Details

**Materials and Specimens.** Carbon steels JIS SK5 and SK3 are used in the experiment. The chemical composition is (mass percent,%): C 0.83(1.10), Si 0.20(0.29), Mn 0.39(0.42), P 0.016(0.017) and S 0.005(0.008). Specimens used for the experiment are 60 mm in length, 10mm in width and 3mm in thickness. The specimens are spheroidizing annealed to form cementite particles with large (SL) and

small (SS) spheroidal structures [2]. Final micrographs and mechanical properties of four different kinds of specimen are listed in Table 1.

Table 1 Mechanical properties and micrograph of the specimen

Specimen	Material	$f$ (%)	$d$ ( $\mu\text{m}$ )	$E$ (Gpa)	$\sigma_y$ (MPa)	HV	Micrograph
1#	SK5-SL	13.1 $\pm$ 0.1	2.0~3.0	189	327	163	Fig.(a)
2#	SK5-SS	13.8 $\pm$ 0.2	0.5~1.0	197	477	192	Fig.(b)
3#	SK3-SL	16.0 $\pm$ 0.1	2.0~4.0	183	364	170	Fig.(c)
4#	SK3-SS	15.0 $\pm$ 0.3	0.5~1.5	187	415	175	Fig.(d)

Note:  $f$ -Volume fraction of cementite particle;  $d$ -Diameter of cementite particle;  $E$ -Mechanical Young's modulus;  $\sigma_y$ -Yield stress; HV-Vickers hardness.

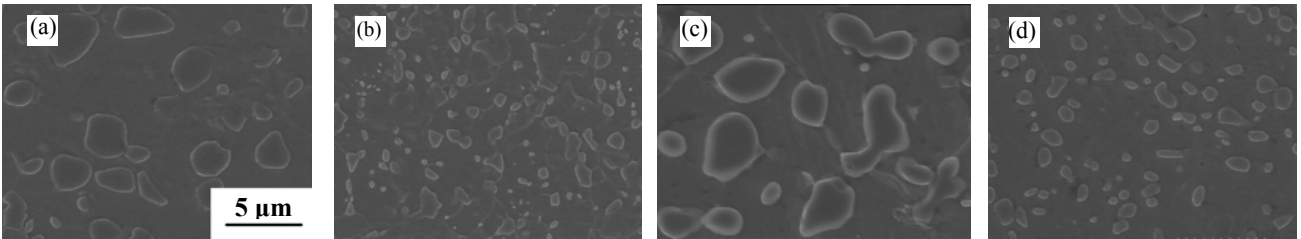


Table 2 Mechanical and thermal properties of two phases [6]

	Young's modulus (GPa)	Poisson's ratio	Coefficient of thermal exp. ( $\times 10^{-6} \text{ } ^\circ\text{C}^{-1}$ )
Ferrite	206	0.28	12
Cementite	280	0.23	17

**Modeling Procedure.** The computation simulations are done via OOF2, software which applies the finite element method at the microscale, by using microstructural images and materials properties as input data [7, 8]. It reads these images, assigns material properties to features in the image, and directly creates two-dimensional finite element meshes on them. Finally, the FEM solver conducts virtual experiments to determine the macroscopic properties of the microstructure. In the present work, simulation models used are built on the micrographs shown in Table 1, the ferrite and the cementite phases are identified and the corresponding materials were assigned according to Table 2. Finally, the finite triangle element mesh is created. The meshes are adaptive, i.e. the mesh is refined at the ferrite/cementite particle interface, where the stresses present the highest concentration. Fig.1

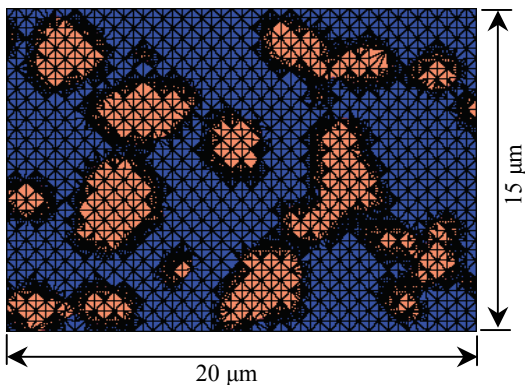


Figure 1 Finite element mesh created from micrograph

shows an example of created finite element mesh. To determine the stress evolutions under the elastic deformation, uniaxial tensile stresses, which are 80, 160 and 240 MPa, are applied in the transverse direction. In addition, to investigate thermal stresses in the composite arising from the mismatch in the thermal expansion coefficient (as listed in Table 2), a gradient of temperature from room temperature to 500°C is also required as input in the numerical model.

**X-ray Stress Measurement.** The *in situ* four-point bending test is conducted to determine the characteristics of the stress distribution in the ferrite and cementite phases. The stresses in two phases are measured axially to the applied loading direction of the specimens. Before the X-ray measurement, the specimen surface is treated previously as described in our previous paper [2]. The ferrite and

cementite peaks are scanned with a scintillation detector at 30kV and 10mA. Stress measurements are made with chromium radiation using the 211 diffraction peak at approximately 156 deg  $2\theta$  for the ferrite phase and the 250 peak at approximately 148 deg  $2\theta$  for the cementite phase.

## Results and Discussion

Stress evolutions in the cementite and the ferrite phases under the uniaxial tensile loading that calculated via OOF code are shown in Fig.2. In all specimens, it is observed that stresses in the cementite are higher those in the ferrite, and stresses in both phases increase with increasing applied macroscopic stress. In Fig.2 (a), Specimen 1 and Specimen 3 have the similar particle size but cementite volume fraction of Specimen 3 is higher than that of Specimen 1. It shows that stresses in Specimen 1 are higher than those in Specimen 3 for the cementite phase, but almost no stress difference between the two specimens is found for the ferrite phase. In Fig.2 (b), Specimen 1 and Specimen 2 have a similar cementite volume fraction but particle size of Specimen 2 is higher than that of Specimen 1. For the cementite phase, stresses in Specimen 2 are found to be higher than those in Specimen 1, but almost no stress difference between the two specimens is found for the ferrite phases. The relationships observed in Fig.2 (c) are the same with those observed in the Fig.2 (b).

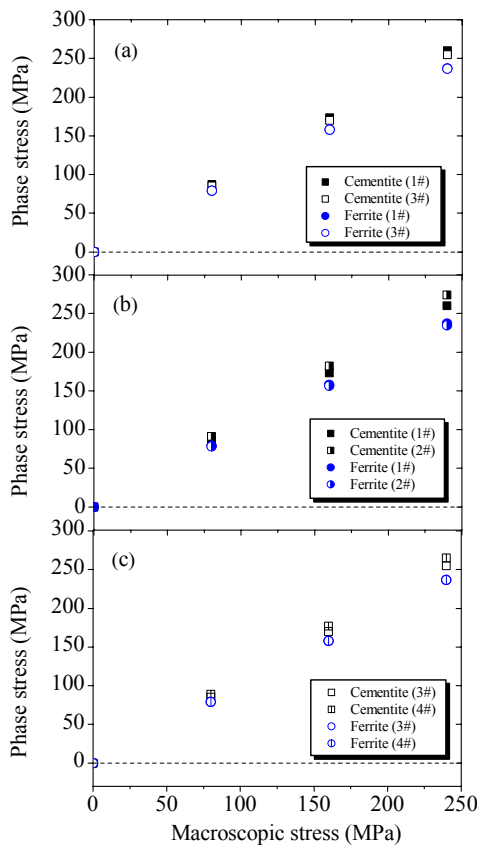


Figure 2 Phase stress calculated using OOF

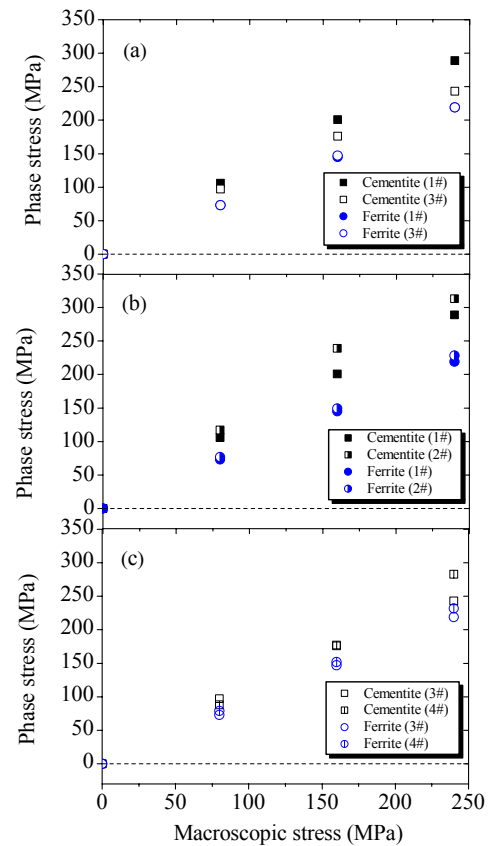


Figure 3 Phase stress evolutions measured by X-ray

Fig.3 shows X-ray measured stress evolutions of the ferrite and the cementite in the *in situ* four-point bending experiment. For the cementite, it indicates that the stress relationships observed by experiment are the same with the computational ones. For the ferrite, the experimental results show that stresses in Specimen 2 are higher than those in Specimen 1 [Fig.3 (b)], and stresses in Specimen 4 are higher than those in Specimen 3 [Fig.3 (c)]. In the calculations, however, these differences are not obviously observed. It is possible to explain this phenomenon by considering the additional rate of work hardening that induced in the SS specimen. Because the quenching process in the heat treatment for making SS specimen reduces grain size of the ferrite, and induces the rate of work hardening in the SS specimen is higher than that in the SL specimen. This part of work hardening, however, is not considered in the OOF calculations.

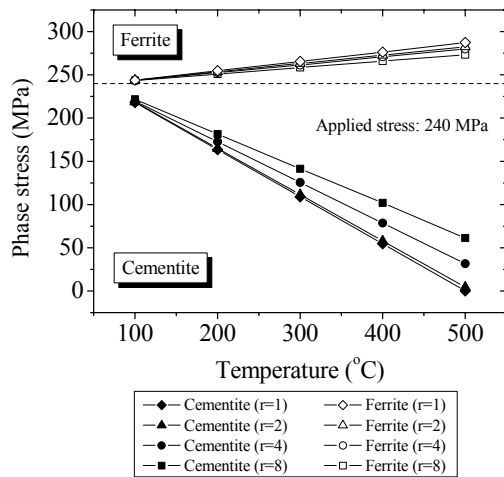


Figure 4 Stresses under the thermo-mechanical loading, calculated by the generated model with  $f = 15\%$  and different relative size  $r$ .

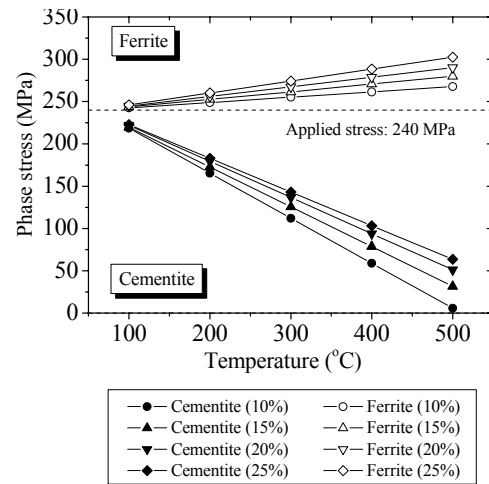


Figure 5 Stresses under the thermo-mechanical loading, calculated by the generated model with a relative size  $r=4$  and different  $f$ .

In present study, the effect of environmental temperature on the stress state of specimen that is under a mechanical loading is investigated. To discuss effects of the microstructure of the cementite on the stress evolutions using OOF, micrographs containing various content spherical cementite particles, which have a relative size of 1, 2, 4 and 8, are randomly generated. Fig.4 shows the dependence of the stress evolutions on the particle size of the cementite under the thermo-mechanical loading. For a given volume fraction of the cementite particle, it shows that the stress in the ferrite increases but the stress in the cementite decreases, with increasing the surrounding temperature. For a given surrounding temperature, the stress in the ferrite increases but the stress in the cementite decreases, with decreasing the particle size of the cementite. In both the ferrite and the cementite, the slopes of the curves increase with decreasing the particle size of the cementite. Fig.5 shows the dependence of the stress evolutions on the volume fraction of the cementite particle under the thermo-mechanical loading. For a given particle size of the cementite, it indicates that the stress in the ferrite increases but the stress in the cementite decreases, with increasing the surrounding temperature. For a given surrounding temperature, the stresses in both the ferrite and the cementite increase with increasing the volume fraction of the cementite. Furthermore, the slope of the curve for the ferrite increases, however, that for the cementite decreases with increasing the volume fraction of the cementite,

## Summary

In this paper, the effect of microstructure on the internal stress states of steels under the mechanical and thermo-mechanical loadings are analyzed using the finite element method. For the steels SK5 and SK3, numerical models based on finite element simulations of the material's real microstructures are considered. The computational results are compared with the experimental results. The comparison indicates that the model is suitable for analyzing the effects of the particle size and volume fraction of the cementite on the stress states of carbon steels.

## References

- [1] L.S. Darken and R.W. Gurry: *AIME Trans.*, (1951), p.1015
- [2] L. Che, M. Gotoh and Y. Horimoto et al.: *Mat. Sci. For.*, Vol. 524-525 (2006), p.943
- [3] K. Tohgo, H. Ishii and K. Hiramatsu et al.: *Jpn. Soc. Mech. Eng.*, Vol.59A (1993), p.43
- [4] W.S. Lee, C.Y. Liu: *Mater. Sci. Eng.*, Vol.426A (2006), p.101
- [5] C.R.S. da Silva, M. Boccalini: *Mater. Sci. Tech.*, Vol.21 (2005), p.565
- [6] W.W. Webb, W.D. Forgeng: *Acta Metall.*, Vol.6 (1958), p.462
- [7] S.A. Langer, Jr. Fuller and E.R. Carter: *Comput. Sci. Eng.*, Vol.3(3) (2001), p.15
- [8] S.A. Langer, A. Reid and S-I. Haan et al: *The OOF2 Manual*, Version 2.0, (2006)